engineering proceedings

Proceeding Paper

A Multifractal-Based Structural Representation of Retinal Images for Diabetic Retinopathy Analysis †

Hajar Karkri [1,*], Ali El Moussati [1], Yassine Ayat [2], Oumayma Rachdi [1] and Maryem Dinar [1]

[1] IASCA Research Group, Laboratory of Engineering Sciences and Intelligent Systems, National School of Applied Sciences Oujda, Mohammed First University, Oujda 60000, Morocco; a.elmoussati@ump.ac.ma (A.E.M.); oumayma.rachdi.d24@ump.ac.ma (O.R.); maryem.dinar.d25@ump.ac.ma (M.D.)
[2] SEIMC Research Group, LASMAR, Higher School of Technology Meknes, Moulay Ismail University, Meknes 50000, Morocco; yassine.ayat@ump.ac.ma
* Correspondence: hajar.karkri.d24@ump.ac.ma
† Presented at the 13th International Electronic Conference on Sensors and Applications, 18–20 November 2026; Available online: https://sciforum.net/event/ECSA-13.

Abstract

Retinal damage caused by diabetes develops silently, and patients generally become aware of a problem only once their vision has deteriorated. Early automated detection therefore represents a concrete medical priority. Yet, a central question remains rarely addressed: are the image representations used by these systems actually designed for this purpose? Methods such as Contrast Limited Adaptive Histogram Equalization (CLAHE), histogram equalization, and gamma correction are widely used, but their primary objective is to improve image appearance rather than characterize the structural changes associated with different stages of diabetic retinopathy (DR). To address this limitation, this work introduces a multifractal geometry-based framework for retinal image representation and DR analysis. The framework consists of three main parts. First, normal anatomical structures, including blood vessels and the optic disc, are removed. Second, local variations in retinal structural regularity are estimated across different spatial scales. Third, multifractal maps are generated to represent local structural alterations in the retina. The removal of dominant anatomical structures focuses the analysis on the remaining retinal regions, while the multiscale analysis characterizes spatial variations in retinal structure associated with disease progression. Experiments performed on the Messidor-2 dataset showed stronger stage-related variations in multifractal maps than in CLAHE-enhanced images. The eta-squared analysis showed a stronger association between the extracted features and the severity of DR, with values reaching up to 0.955 for multifractal maps. In addition, the overall separation between DR severity stages improved from −0.032 for CLAHE-enhanced images to 0.293 for multifractal maps, indicating a better distinction between severity stages. The key novelty lies in a lesion-centered multifractal representation that accounts for retinal structural complexity, thereby connecting multifractal analysis with intelligent systems for automated diabetic retinopathy grading.

Keywords: diabetic retinopathy; intelligent systems; retinal structural complexity; multifractal maps

Check for updates

Academic Editor: Francisco Falcone

Published: 26 October 2026

Copyright: © 2026 by the authors. Licensee MDPI, Basel, Switzerland. This article is an open access article distributed under the terms and conditions of the Creative Commons Attribution (CC BY) license.

1. Introduction

Diabetic retinopathy (DR) is a leading cause of preventable blindness and vision impairment worldwide, affecting approximately 103.12 million adults in 2020. This number

is projected to increase to 160.50 million by 2045 due to the rising global prevalence of diabetes [1]. The disease progresses silently, pathological changes gradually accumulating in the retinal tissue long before visual symptoms become apparent [2,3]. As a result, many patients are diagnosed only after irreversible damage to the retina has occurred, at which point therapeutic interventions are less effective. The progression of this disease calls for the development of accurate and automatic screening systems that are able to detect DR in its early stages, especially in areas with limited access to ophthalmological specialists.

Recent advances in artificial intelligence, especially deep learning, have significantly improved computer-aided diagnosis (CAD) systems for retinal image analysis. Nevertheless, the performance of these models largely depends on the quality of the image representation provided as input [4]. To improve the visibility of retinal structures, image preprocessing techniques such as Contrast Limited Adaptive Histogram Equalization (CLAHE), gamma correction are almost systematically applied before feature extraction by convolutional neural networks (CNNs).

These enhancement strategies have been shown to be effective in several studies, but each of them targets only a narrow aspect of the DR characterisation. Naz and Ahuja [5] proposed a hybrid MdFCM-SVM classifier for microaneurysm detection using HSI color transformation, median filtering, histogram equalisation and morphological optic disc removal. However, the framework is focused on a single lesion type, instead of the whole range of DR related changes. Macsik et al. [6] compared several variants of CLAHE (min-pooling, RGB, Lab, MaxGreenGsc) in an ensemble of Xception and EfficientNetB4, improving classification accuracy through hard and soft voting at the cost of significantly higher computational complexity. Rahman et al. [7] achieved 98.81% accuracy with a hybrid 6L-ConvSVM-RF classifier based on YOLO lesion segmentation and modified CLAHE but with a binary severity classification, not fine-grained clinical grading. Sarki et al. [8] suggested a pipeline that combines CLAHE, Tyler Coye vessel segmentation, Circular Hough optic disk localization and Otsu-based exudate detection to achieve 93.33% accuracy with a custom CNN. However, the pretrained models tested were limited to using the default, non-optimized hyperparameters. Boulaabi et al. [9] applied image cropping, CLAHE enhancement, data augmentation and a Swin Transformer architecture with shifted-window self attention. They achieved 89.65% accuracy on APTOS and 97.40% on IDRiD, which shows a significant strength on early stage DR.

Overall, conventional retinal image preprocessing methods are mainly designed to improve contrast and enhance the visibility of retinal structures. However, they provide limited information about the spatial and structural changes that occur with diabetic retinopathy (DR) progression. As DR severity increases, pathological manifestations such as microaneurysms, hemorrhages, exudates, and neovascularization introduce increasingly heterogeneous and irregular patterns within the retina.

Multifractal analysis offers an alternative representation by characterizing local structural variations across multiple spatial scales. In this study, a multifractal-based approach is proposed to represent DR-related retinal variations beyond conventional intensity enhancement. After removing the retinal vessels and optic disc, local multifractal properties are estimated to generate spatial maps reflecting variations in retinal structure.

The proposed representation is evaluated on Messidor-2 across the five DR severity stages and compared with CLAHE-enhanced images using statistical and texture descriptors. One-way ANOVA, eta-squared η^2, and the Silhouette Score are employed to quantify stage-related variability and overall separability. The following sections describe the methodology, present and discuss the experimental findings, and summarize the main conclusions.

https://doi.org/10.3390/engproc2026163004

2. Materials and Methods

2.1. Dataset

The retinal fundus images used in this study are taken from the Messidor-2 dataset, a publicly available dataset generated for the purpose of computer-assisted diagnosis of diabetic retinopathy (DR). The dataset contains 1748 macula-centered color fundus images from 874 examinations. The images are acquired with a 45° field of view and are provided in different image resolutions and formats [10].

For diabetic retinopathy grading, third-party annotations available for 1744 images are considered. The images are labeled into five classes based on the presence and severity of DR: No DR (Grade 0), Mild Non-Proliferative Diabetic Retinopathy (Mild NPDR, Grade 1), Moderate Non-Proliferative Diabetic Retinopathy (Moderate NPDR, Grade 2), Severe Non-Proliferative Diabetic Retinopathy (Severe NPDR, Grade 3) and Proliferative Diabetic Retinopathy (PDR, Grade 4). The class distribution consists of 1017 images for Grade 0, 270 for Grade 1, 347 for Grade 2, 75 for Grade 3, and 35 for Grade 4. Grade 0 refers to retinal images without any signs of diabetic retinopathy, and Grades 1–4 refer to the progressive stages of the disease from mild NPDR to proliferative DR, as shown in Figure 1. The selected retinal fundus images are processed through the proposed pipeline comprising preprocessing, anatomical structure segmentation and multifractal analysis.



(**a**) (**b**) (**c**) (**d**) (**e**)

Figure 1. Representative retinal fundus images from the Messidor-2 dataset: (**a**) No DR, (**b**) Mild NPDR, (**c**) Moderate NPDR, (**d**) Severe NPDR, and (**e**) PDR.

2.2. Data Preprocessing

The Messidor 2 dataset consists of retinal fundus images acquired under different conditions and consequently exhibits variations in illumination, contrast, and overall image quality. Therefore, a preprocessing stage is carried out to prepare the images for the subsequent steps of the proposed approach.

The dataset firstly examined to identify and remove images that are unsuitable for further analysis. Completely black images and images containing insufficient retinal information are excluded. After this quality screening, the retained images are enhanced using Contrast Limited Adaptive Histogram Equalization (CLAHE). This method enhances local contrast and overcomes the problem of over-amplification which can increase the visibility of retinal structures. The enhanced fundus images were then fed as input to the segmentation stage.

2.3. Retinal Anatomical Structure Segmentation

Following the preprocessing stage, the retinal fundus images are segmented to identify the blood vessels and optic disc. This step is performed before the multifractal analysis to remove these major anatomical structures and focus the subsequent analysis on the remaining retinal regions.

Blood vessels segmentation is performed using a pre-trained Attention U-Net taken from an open-source implementation of retinal vessels segmentation [11], trained and tested on DRIVE, STARE, and HRF datasets and selected for its best reported overall performance

(accuracy/mean IoU of 0.905/0.745, 0.893/0.738, and 0.966/0.857, respectively). Optic disc segmentation is performed using a pre-trained model from the joint optic disc and cup segmentation approach of Fu et al. [12], developed on the ORIGA dataset with 0.983 accuracy for optic disc segmentation.

Both pre-trained models are applied to the Messidor-2 images to generate the corresponding vessels and optic disc masks. Since ground-truth masks are unavailable for Messidor-2, segmentation quality is assessed using four unsupervised criteria [13]: LEV1 (intra-region homogeneity), ZEB (intra-region uniformity combined with inter-region contrast), ROS1 (joint intra- and inter-region information), and ROS2 (adapted intra-/inter-region disparity for uniform vs. textured regions). As presented in Tables 1 and 2, all four criteria remained stable across the five DR severity stages for both vessels and optic disc segmentation, with no systematic deterioration observed with increasing disease severity. This consistency allows for the use of the generated masks for the removal of anatomical structures before multifractal analysis.

Table 1. Unsupervised evaluation of retinal blood vessels segmentation across the five DR severity stages.

DR Stage	LEV1	ZEB	ROS1	ROS2
No DR	0.964	0.416	0.482	0.435
Mild	0.960	0.429	0.477	0.377
Moderate	0.959	0.408	0.478	0.390
Severe	0.956	0.381	0.476	0.393
PDR	0.962	0.338	0.483	0.450

Table 2. Unsupervised evaluation of optic disc segmentation across the five DR severity stages.

DR Stage	LEV1	ZEB	ROS1	ROS2
No DR	0.950	0.423	0.535	0.661
Mild	0.946	0.412	0.532	0.681
Moderate	0.944	0.392	0.531	0.677
Severe	0.943	0.316	0.528	0.679
PDR	0.953	0.364	0.535	0.645

2.4. Multifractal Analysis

Multifractal analysis is a mathematical approach used to characterize the spatial complexity and local variations of heterogeneous patterns across multiple scales [14]. It provides a quantitative description of how the structural properties of an image vary from one region to another and across different observation scales.

In retinal fundus images, pathological features associated with diabetic retinopathy, such as microaneurysms, hemorrhages, and exudates, produce local variations in intensity, texture, and spatial organization. Moreover, these lesions may appear at different sizes and locations across the retina. Multifractal analysis is therefore used to characterize these heterogeneous retinal patterns over multiple spatial scales. In the present study, the analysis is applied to the preprocessed fundus images after the removal of the blood vessels and optic disc, allowing the remaining retinal regions to be investigated.

The multifractal analysis is based on a multiscale box-partitioning approach [15]. The retinal image is divided into boxes of different sizes ε, where each box represents a local region of the image. The use of different box sizes allows image information to be analyzed at different spatial scales. Small boxes describe fine and localized variations, whereas larger

boxes capture broader retinal patterns. For each box i at scale ε, the image information contained within the box is used to calculate a normalized measure $p_i(\varepsilon)$:

$$p_i(\varepsilon) = \frac{n_i(\varepsilon)}{\sum_j n_j(\varepsilon)} \tag{1}$$

where $n_i(\varepsilon)$ represents the image mass within the i-th box. The normalized measures describe how the image information is distributed among the different boxes. To characterize this distribution for different moment orders q, a q-dependent normalized measure is defined as:

$$\mu_i(q, \varepsilon) = \frac{p_i^q(\varepsilon)}{\sum_j p_j^q(\varepsilon)} \tag{2}$$

The moment order q controls the contribution of regions with different image measures to the multifractal analysis. By varying q, different components of the image distribution can therefore be characterized.

The local scaling behavior is then described by the Hölder exponent $\alpha(q)$, estimated across the different observation scales as:

$$\alpha(q) = \lim_{\varepsilon \to 0} \frac{\sum_i \mu_i(q, \varepsilon) \log p_i(\varepsilon)}{\log \varepsilon} \tag{3}$$

The estimated Hölder exponent $\alpha(q)$ is used to create a multifractal map describing the spatial distributions of local retinal complexity. These maps are built for different stages of diabetic retinopathy (No DR, Mild, Moderate, Severe and Proliferative DR) to characterize and compare the heterogeneous retinal patterns associated with disease progression.

2.5. Multifractal Map Generation Procedure

Figure 2 illustrates the main steps of multifractal map generation from the preprocessed retinal image. The map is constructed through a patch-based analysis that captures spatial variations in retinal complexity. The preprocessed image is first divided into overlapping patches, and the singularity exponents $\alpha(q)$ are estimated independently within each patch. The corresponding spectrum width, defined as $\Delta\alpha = \alpha_{\max} - \alpha_{\min}$, is then calculated and used as the representative multifractal value of each patch. The resulting $\Delta\alpha$ values are assigned to their corresponding spatial locations to form an initial map. The map is resampled to the original resolution of the image and smoothed to ensure spatial continuity. Robust normalization and retinal field-of-view masking are applied to reduce the influence of extreme values and restrict the representation to the retinal region. The final $\Delta\alpha$ map thus provides a spatial representation of local multifractal variations across the retina.

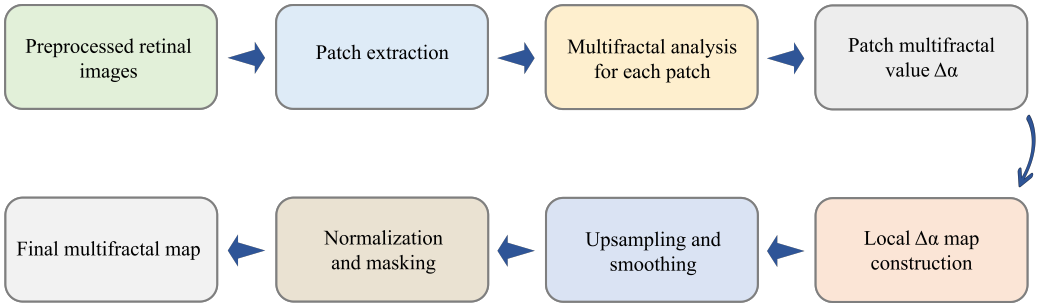


Figure 2. Main steps involved in the generation of the multifractal $\Delta\alpha$ map.

3. Results

The experimental results were evaluated to determine how effectively the multifractal representation captures retinal variations across the five DR severity stages. Representative multifractal maps were first examined to illustrate stage-related changes in retinal patterns. A quantitative comparison with CLAHE-enhanced images was then performed using six statistical and texture features, while one-way ANOVA, eta-squared η^2, and the Silhouette Score were used to assess feature variability and overall stage separability.

3.1. Multifractal Maps Across Diabetic Retinopathy Stages

Figure 3 presents representative multifractal maps obtained for the five diabetic retinopathy (DR) stages considered in this study: No DR, Mild NPDR, Moderate NPDR, Severe NPDR, and Proliferative DR (PDR). The generated maps provide a spatial representation of the local multifractal variations within the retinal images after preprocessing and removal of the main anatomical structures.

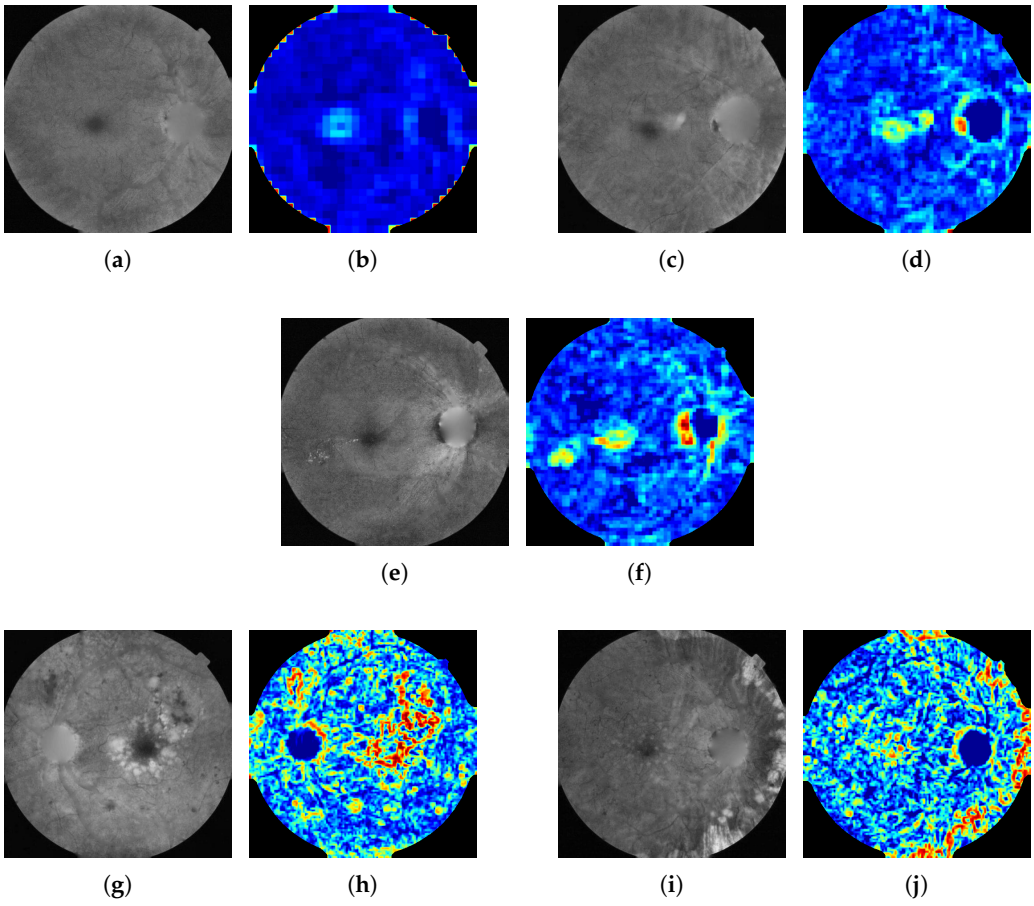


Figure 3. Comparison of CLAHE-enhanced images and multifractal maps across DR severity stages: (**a**,**b**) No DR, (**c**,**d**) Mild NPDR, (**e**,**f**) Moderate NPDR, (**g**,**h**) Severe NPDR, and (**i**,**j**) PDR. For each stage, the first image corresponds to the CLAHE-enhanced image and the second to the multifractal map.

A visual examination of these maps reveals different spatial patterns according to the DR stage. The No DR images generally exhibit relatively homogeneous multifractal patterns, whereas the pathological stages show progressively more heterogeneous and spatially irregular distributions. These variations reflect changes in the local texture and structural complexity of retinal regions associated with the presence and progression of pathological alterations. The multifractal representation therefore provides a complemen-

tary visualization in which local variations that are less distinguishable in conventional intensity-based images can be emphasized.

3.2. Statistical Assessment of Feature Discrimination and Class Separability

Statistical analysis showed significant differences in the capacity of multifractal maps and CLAHE-enhanced images for characterizing variability through the five DR phases (see Table 3). For CLAHE, all features except Entropy exhibited significant differences over DR stages ($p < 0.05$); yet, the corresponding effect sizes were low ($\eta^2 = 0.005$–0.077), suggesting that DR stage accounted for only a small part of the variation in features. In contrast, all features extracted from the multifractal maps differed significantly across DR stages ($p < 0.05$) and exhibited substantially higher effect sizes ($\eta^2 = 0.457$–0.955). The strongest stage-related variations were observed for GLCM (Gray-Level Co-occurrence Matrix) Homogeneity ($\eta^2 = 0.955$), GLCM Contrast ($\eta^2 = 0.869$), and CV (Coefficient of Variation) ($\eta^2 = 0.811$). These results indicate that the statistical and texture properties of the multifractal maps vary more strongly with DR severity than those derived from CLAHE-enhanced images.

The overall feature-space analysis showed a similar trend. CLAHE resulted features produced a negative Silhouette Score of -0.032, demonstrating substantial overlap in the five DR stages while the multifractal features achieved a positive score of 0.293, indicating better but not yet completed stage division. In general, the larger effect sizes and higher silhouette score suggest that the multifractal representation gives a more pronounced characterization of retinal variations across DR stages was better than CLAHE enhancement.

Table 3. Statistical comparison of CLAHE-enhanced images and multifractal maps across the five diabetic retinopathy stages using one-way ANOVA and eta-squared (η^2).

Feature	CLAHE p	CLAHE η^2	Multifractal p	Multifractal η^2
Entropy	0.084	0.005	<0.05	0.689
CV	<0.05	0.021	<0.05	0.811
Contrast	<0.05	0.077	<0.05	0.869
Homogeneity	<0.05	0.054	<0.05	0.955
Energy	<0.05	0.018	<0.05	0.737
Correlation	<0.05	0.030	<0.05	0.457

4. Discussion

The results demonstrate that multifractal maps provide a more stage-sensitive representation of retinal variations than CLAHE-enhanced images. The consistently higher η^2 values obtained for the multifractal features indicate that their variability is more strongly associated with DR severity. This finding supports the initial hypothesis that a representation based on local scale-dependent properties can better characterize disease-related retinal variations than conventional contrast enhancement.

The strongest effects were observed for GLCM Homogeneity ($\eta^2 = 0.955$), Contrast ($\eta^2 = 0.869$) and CV ($\eta^2 = 0.811$), suggesting that changes in local similarity, heterogeneity and relative dispersion within the multifractal maps mainly reflect the DR progression. However, the small effect sizes for CLAHE-enhanced images suggest that local contrast enhancement alone provides little characterization of stage-related structural differences. This is because the two methods have different goals: CLAHE increases the visibility of the image by changing the local intensity distributions, while multifractal analysis describes the heterogeneous patterns and local scaling behavior at several spatial scales.

These findings are consistent with previous studies showing the relevance of fractal and multifractal approaches for characterizing complex retinal structures and pathological

changes [14]. The present study extends this perspective by representing local multifractal variations spatially and evaluating their association with the five DR severity stages. The improvement in Silhouette Score from −0.032 for CLAHE to 0.293 for multifractal maps further supports this observation, although the remaining overlap indicates that the stages are not completely separated.

The overall results point to the potential of multifractal maps to characterize retinal variations as a function of DR severity. However, this study was done on one retinal dataset and the results are not generalizable. Future work should thus validate the proposed representation on independent retinal datasets acquired under different imaging conditions, and further explore the relation between multifractal patterns and specific DR manifestations such as microaneurysms, hemorrhages and exudates.

5. Conclusions

The results of this study showed that the application of the multifractal analysis is more informative than CLAHE enhancement for the characterization of the retinal variations at different stages of DR severity. The multifractal maps generated higher effect sizes and better stage separability, signifying they are more responsive to structural changes linked to the disease. The results show the potential of multifractal maps to characterize the changes associated with the DR progression. In future work, the evaluation will be extended to independent retinal datasets and the relation of multifractal patterns to specific DR-related changes will be further explored.

Author Contributions: Conceptualization, H.K. and A.E.M.; methodology, H.K.; software, H.K.; validation, H.K., A.E.M., Y.A., O.R. and M.D.; formal analysis, H.K.; investigation, H.K.; data curation, H.K.; writing—original draft preparation, H.K.; writing—review and editing, H.K., A.E.M., Y.A., O.R. and M.D.; visualization, H.K.; supervision, A.E.M.; project administration, A.E.M. All authors have read and agreed to the published version of the manuscript.

Funding: This research received no external funding.

Institutional Review Board Statement: Not applicable.

Informed Consent Statement: Not applicable.

Data Availability Statement: The data used in this study are publicly available from the Messidor-2 dataset.

Acknowledgments: During the preparation of this manuscript, the authors used ChatGPT (OpenAI, GPT-5.6) for the purposes of language editing and improving the clarity and readability of the text. The authors have reviewed and edited the output and take full responsibility for the content of this publication.

Conflicts of Interest: The authors declare no conflicts of interest.

Abbreviations

The following abbreviations are used in this manuscript:

HSI	Hue, Saturation, Intensity
RGB	Red, Green, Blue
MdFCM-SVM	Modified Fuzzy C-Means–Support Vector Machine
6L-ConvSVM-RF	Six-Layer Convolutional Support Vector Machine–Random Forest
YOLO	You Only Look Once
APTOS	Asia Pacific Tele-Ophthalmology Society
IDRiD	Indian Diabetic Retinopathy Image Dataset
DRIVE	Digital Retinal Images for Vessel Extraction
STARE	Structured Analysis of the Retina

HRF	High-Resolution Fundus
IoU	Intersection over Union
ORIGA	Online Retinal Fundus Image Database for Glaucoma Analysis
LEV1	Levine Criterion 1
ZEB	Zeboudj Criterion
ROS1	Rosenberger Criterion 1
ROS2	Rosenberger Criterion 2
ANOVA	Analysis of Variance
GLCM	Gray-Level Co-occurrence Matrix
CV	Coefficient of Variation

References

1. Teo, Z.L.; Tham, Y.C.; Yu, M.; Chee, M.L.; Rim, T.H.; Cheung, N.; Bikbov, M.M.; Wang, Y.X.; Tang, Y.; Lu, Y.; et al. Global Prevalence of Diabetic Retinopathy and Projection of Burden through 2045: Systematic Review and Meta-analysis. *Ophthalmology* **2021**, *128*, 1580–1591. [CrossRef] [PubMed]
2. Karkri, H.; El Moussati, A.; Kpalma, K. Enhanced Binary Detection of Diabetic Retinopathy Using a Two-stage Transfer Learning Framework. *Int. J. Comput. Digit. Syst.* **2026**, *19*. [CrossRef]
3. Karkri, H.; El Moussati, A.; Ayat, Y.; Rachdi, O.; Abdelouahab, M. Multi-class Classification for Diabetic Retinopathy Detection Using Fine-Tuned Xception Model. *Lect. Notes Netw. Syst.* **2026**, *1924*, 205–216. [CrossRef]
4. Grzybowski, A.; Jin, K.; Zhou, J.; Pan, X.; Wang, M.; Ye, J.; Wong, T.Y. Retina Fundus Photograph-Based Artificial Intelligence Algorithms in Medicine: A Systematic Review. *Ophthalmol. Ther.* **2024**, *13*, 2125–2149. . [CrossRef] [PubMed]
5. Naz, H.; Ahuja, N.J. A novel contrast enhancement technique for diabetic retinal image pre-processing and classification. *Int. Ophthalmol.* **2025**, *45*, 11. [CrossRef] [PubMed]
6. Macsik, P.; Pavlovicova, J.; Kajan, S.; Goga, J.; Kurilova, V. Image preprocessing-based ensemble deep learning classification of diabetic retinopathy. *IET Image Process.* **2024**, *18*, 807–828. [CrossRef]
7. Rahman Ema, R.; Chandra Shill, P. Multi-model approach for precise lesion localization and severity grading for diabetic retinopathy and age-related macular degeneration. *Front. Comput. Sci.* **2025**, *7*, 1497929. [CrossRef]
8. Sarki, R.; Ahmed, K.; Wang, H.; Zhang, Y.; Ma, J.; Wang, K. Image Preprocessing in Classification and Identification of Diabetic Eye Diseases. *Data Sci. Eng.* **2021**, *6*, 455–471. [CrossRef] [PubMed]
9. Boulaabi, M.; Gader, T.B.A.; Echi, A.K.; Bouraoui, Z. Enhancing DR Classification with Swin Transformer and Shifted Window Attention. *Lect. Notes Comput. Sci.* **2025**, *15735*, 57–61. [CrossRef] [PubMed]
10. Kaggle. Messidor-2. Available online: https://www.kaggle.com/datasets/mariaherrerot/messidor2preprocess (accessed on 19 August 2026).
11. Sarkar, A. Retinal Vessel Segmentation Using Variants of U-Net. GitHub Repository, 2021. Available online: https://github.com/arkanivasarkar/Retinal-Vessel-Segmentation-using-variants-of-UNET (accessed on 28 August 2026).
12. Fu, H.; Cheng, J.; Xu, Y.; Wong, D.W.K.; Liu, J.; Cao, X. Joint Optic Disc and Cup Segmentation Based on Multi-Label Deep Network and Polar Transformation. *IEEE Trans. Med. Imaging* **2018**, *37*, 1597–1605. [CrossRef] [PubMed]
13. Chabrier, S.; Emile, B.; Rosenberger, C.; Laurent, H. Unsupervised performance evaluation of image segmentation. *EURASIP J. Appl. Signal Process.* **2006**, *2006*, 096306. [CrossRef]
14. Yang, L.; Zhang, M.; Cheng, J.; Zhang, T.; Lu, F. Retina images classification based on 2D empirical mode decomposition and multifractal analysis. *Heliyon* **2024**, *10*, e27391. [CrossRef] [PubMed]
15. Yao, B.; Imani, F.; Sakpal, A.S.; Reutzel, E.; Yang, H. Multifractal Analysis of Image Profiles for the Characterization and Detection of Defects in Additive Manufacturing. *J. Manuf. Sci. Eng. Trans. ASME* **2018**, *140*, 031014. [CrossRef]

Disclaimer/Publisher's Note: The statements, opinions and data contained in all publications are solely those of the individual author(s) and contributor(s) and not of MDPI and/or the editor(s). MDPI and/or the editor(s) disclaim responsibility for any injury to people or property resulting from any ideas, methods, instructions or products referred to in the content.